Date of Report: 22/11/2024
Date of Experiment:11/11/2024

Gamma Radiation

Experiment conducted by Berk Batin ARI
Lab Partner was Daren ZHENG

Abstract

In this report, gamma radiation from four isotopes—Cesium (Cs-137), Sodium (Na-22), Americium (Am-241), and Cobalt (Co-60)—was investigated using a Multichannel Analyzer (MCA) in two parts. Initially, the MCA was calibrated using Cs-137 and Am-241, where the proportionality constant was determined as 3.885, and the error in the count number was calculated as $\pm$ 2632.0. Due to experimental setup errors, two additional calibrations were performed, resulting in proportionality constants of 1.9 and 7.8 for Cs-137 and Co-60, respectively. The gamma radiation energies (Eγ) for Am-241 and Cs-137 were measured as 49.05 keV and 609.1 keV, respectively. Additionally, Compton scattering for Cs-137 was found to be 396.3 keV, and its backscattering energy was calculated as 182.6 keV.

In the second part, the Eγ values for Cs-137, Na-22, and Co-60 were measured as 761.7 keV, 1294 keV, and 1554 keV, with associated errors of 15.00%, 10.33%, and 21.84%, respectively. Their Compton scattering energies were calculated as 466.0 keV (error 52.02%) for Cs-137, 1029 keV (error 180.3%) for Co-60, and 975.0 keV (error 153.2%) for Na-22. Backscattering energies were measured as 295.2 keV (error 35.20%) for Cs-137, 265.0 keV (error 71.43%) for Co-60, and 578.0 keV (error 50.53%) for Na-22. The rest mass of the electron was determined to be 5094 ± 1770 keV. Finally, the resolution of the detector was calculated as $0.049 \times 10^{-1} \pm 0.005 \times 10^{-2}$.

These calculations were made by considering the conservation of energy and linear momentum, demonstrating that the energy E transferred to the electron during this process is a function of the scattering angle ϕ.

1. Introduction

Gamma radiation, a high-energy form of electromagnetic radiation, is emitted during the decay of unstable atomic nuclei, typically following alpha or beta decay processes. These high-energy photons are part of the electromagnetic spectrum, positioned beyond X-rays, and are characterised by their extremely short wavelengths (less than ten picometers) and correspondingly high frequencies (greater than $10^{19} Hz$). Due to these properties, gamma radiation possesses significant penetration power, allowing it to traverse materials that would block lower-energy radiation.

This experiment focused on analysing gamma radiation from Cesium (Cs-137), Sodium (Na-22), Americium (Am-241), and Cobalt (Co-60) using a Multichannel Analyzer (MCA), a device that enables the precise measurement of gamma-ray energy spectra.

The Multichannel Analyzer (MCA) was utilized to study the energy spectrum of gamma rays emitted by radioactive isotopes. Electrical signals generated by the detector, such as a scintillation or semiconductor detector, were processed by the MCA. When gamma-ray photons interacted with the detector, voltage pulses proportional to the photons' energy were produced. These pulses were digitized and categorized into discrete energy intervals, referred to as channels, by the MCA. A histogram was constructed, representing the distribution of gamma-ray energies, which allowed key features such as photopeaks, Compton edges, and backscattering peaks to be identified. The calibration process was essential, ensuring that the energy values were accurately correlated with the appropriate channel numbers, thereby enabling precise analysis of the radioactive source's spectral characteristics.

The experiments using MCA need to begin with the calibration of the MCA to establish a proportional relationship between channel number (N) and gamma-ray energy ($E\gamma$), described by:

$$E\gamma = aN + b \tag{1}$$

Where a and b are calibration constants which can be derived from literature values of isotopes, and channel numbers from MCA, this calibration process was critical to ensuring accurate interpretation of the energy spectra, and to calculating unknown sources of radiation. The calibrated MCA would then be used to analyse the gamma radiation from the isotopes. Moreover, Compton edges, backscattering peaks, and photopeaks variables also would be able to be determined with calibration constant by using equation (5).

The interaction of gamma rays with matter primarily occurs via three mechanisms: the photoelectric effect, Compton scattering, and pair production. These interactions depend on the energy of the gamma rays and the atomic number of the target material. Each mechanism plays a distinct role in gamma-ray attenuation and energy transfer. These processes are summarised in **Figure (1)**.

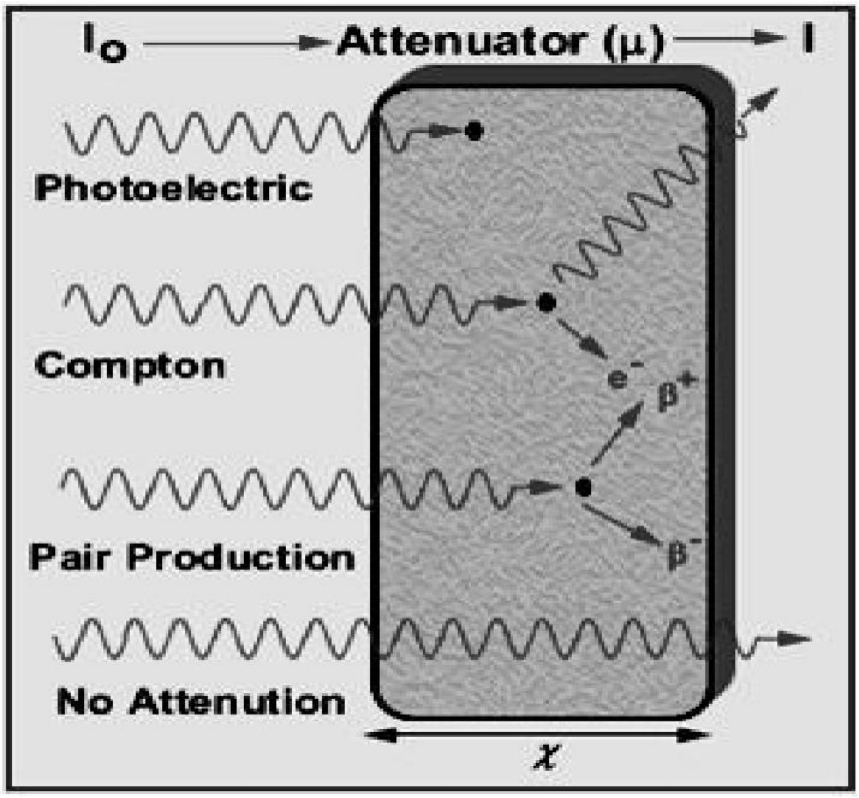

Figure 1: *The primary interactions of gamma rays with matter (Photoelectric effect, Compton scattering, and Pair production. (Molah, A https://www.researchgate.net/figure/Gamma-ray-interaction-mechanism-with-matter_fig1_334993133 , 2019)*

At lower photon energies, the photoelectric effect dominates, where gamma rays transfer their energy entirely to an inner-shell electron, causing its ejection. At intermediate photon energies, Compton scattering occurs, involving the partial transfer of gamma-ray energy to an electron. The scattered photon's energy depends on the scattering angle ϕ and is governed by:

$$\acute{E}_e(\gamma) = \frac{E_\gamma}{1 + \frac{E_\gamma}{m_0 c^2}(1 - \cos\phi)} \qquad (2)$$

The $\acute{E}_e(\gamma)$ the energy of incident gamma-ray, as a function of ϕ , $E_\gamma$is the energy of incident gamma ray, m_0c^2 is the rest mass of an electron. The geometry of Compton scattering is illustrated in **Figure (2)**, showing the relationship between the incident photon, the scattered photon, and the recoiled electron.

"At angle $\phi = \pi$, the scattered $\gamma - ray$ is reflected along its original path. This maximum energy E_c is known as the "Compton edge" since the continuum distribution in the pulse height spectrum looks like a broad plateau that drops rapidly to zero at the energy E_c" *(2024) 5CCP2100 Experimental Physics Laboratory Manual 2024/25*. The equation(3) relates those concept together as

$$\acute{E}_e(\pi) = \frac{E_\gamma}{1 + \frac{m_0c^2}{2E_\gamma}} \tag{3}$$

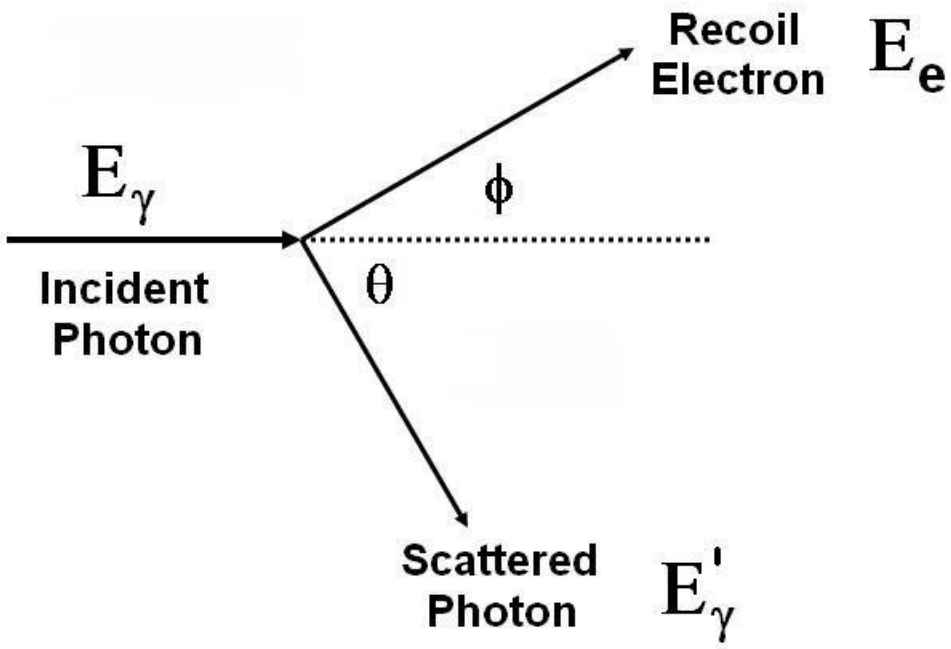

Figure 2: The geometry of Compton scattering, showing the angles of scattering (ϕ) and recoil (θ). *(Veale, M. https://www.researchgate.net/figure/The-geometry-of-Compton-scattering_fig4_236131292 , 2009)*

The shift in wavelength due to scattering is described by the Compton shift equation:

$$\Delta\lambda = \frac{h}{m_0 c}(1 - cos\phi) \tag{4}$$

Backscattering occurs when photons are deflected at angles near $180\ \circ$, creating a distinct peak in the energy spectrum. At higher photon energies exceeding $1.022\ MeV$, pair production becomes significant, involving the conversion of a photon's energy into an electron-positron pair in the presence of a nucleus.

Another key concept of the gamma-ray spectrum is the Full Width at half-maximum (FWHM), which can be calculated as the photo-peak part of the spectrum, and related to that specific part, it can be found by plotting gamma-ray counts versus channel number by using MCA apparatus, and the in the photo-peak section, the total number of gamma-ray counts can be calculated by integration from the starting and ending point of the peak.

Another key feature in the gamma-ray spectrum is the photopeak, which corresponds to the total absorption of a photon's energy. The resolution of the detector at these peaks is quantified using the FWHM:

$$Resolution = \frac{FWHM}{Photopeak\ Energy} \tag{5}$$

indicating the detector's ability to distinguish closely spaced energy levels.

Furthermore, from the relation between the rest mass of an electron and radiation energy, the rest mass of an electron can be found by using equation(3) with an accepted literature value $(511\ keV)$. The relation between Compton scattering edge, backscattering peak and gamma-ray peak can be equated by evaluating equations (2) and (3).

$$E_B = E_\gamma - E_C \tag{6}$$

Where E_B is the backscattering peak and E_C is the Compton scattering edge. This investigation provided detailed insights into the interaction of gamma radiation with matter, emphasising the importance of precise calibration, energy peak analysis, and the physical principles underlying scattering phenomena. The results contribute to a deeper understanding of gamma-ray spectroscopy and its applications.

2. Methods

This investigation was conducted to analyse the gamma radiation emitted by Cesium (Cs-137), Sodium (Na-22), Americium (Am-241), and Cobalt (Co-60) isotopes using a Multichannel Analyzer (MCA). The experimental procedure was divided into two primary sections: calibration and gamma-ray spectral analysis.

Calibration of the MCA

The calibration process was undertaken using Cesium (Cs-137) and Americium (Am-241) isotopes. Each isotope was placed into the MCA detector sequentially, and gamma-ray data were collected for 100 seconds per sample. The high voltage of the detector was adjusted incrementally in steps of 0.03 kV from 0.50 kV to 0.69 kV to optimize signal clarity and identify key spectral features such as the Compton edge, backscattering peak, and photopeak.

The MCA's calibration constant was determined by correlating the channel numbers with the literature energy values of Cs-137 and Am-241 gamma emissions. The proportional relationship between energy (Eγ) and channel number (N) was established using the linear calibration equation (1).

Gamma-Ray Spectral Analysis

In the second section, the gamma-ray spectra of three isotopes—Sodium (Na-22), Cobalt (Co-60), and Cesium (Cs-137)—were measured. Each isotope was inserted into the MCA, and data were recorded over a period of 300 seconds. The resulting spectra were analysed to identify photopeaks, Compton edges, and backscattering regions.

Graphs of the detected gamma-ray intensities versus energy were plotted to facilitate the visual identification of spectral features. These graphs also served as the basis for quantitative analysis, including the determination of gamma-ray energies and their associated errors. The proportionality constant obtained during calibration was applied to calculate the energy values corresponding to the detected gamma emissions.

The standard deviation of the counts' number was calculated to evaluate the variability in the measurements. Error analysis was performed by comparing the experimental results to literature values, as there were no instrumental error sources associated with the MCA during the measurements. All measurements were conducted under controlled environmental conditions to minimize systematic errors. The resolution of the detector and the uncertainties in measurements were carefully analysed to enhance the credibility of the results.

To analyse experimental data, the experiment was plotted and recorded by using special software called CASSY LAB, all settings during the measurements by done by using it.

3. Results

Section 1:

For the first part of the investigation, the calibration was made by plotting the graph as in **Figure(3)** using the linearity of equation(1). Using the arithmetic average equation (7), the proportionality constant was determined as 3.885. The calculation was based on the data when the high voltage was set to 0.63, which gives the best pattern to observe the gamma-ray spectrum for given isotopes in **Figure (8)**. It was also noted that the background noise for each experiment was subtracted from each data value to minimise, and for most of the sections, it was zero.

$$A = \frac{1}{n}\sum_{i=1}^{n} a_i \tag{7}$$

Where A is the arithmetic mean, n is the number of values and a_i and the data set values. The error for the count number was calculated by using the standard deviation equation(8) as 3.01 for the data set, which contributed to the error in the y-axis in **Figure(3).**

$$s = \sqrt{\frac{\sum_{i=1}^{N}(x_i - \bar{x})^2}{N}} \tag{8}$$

Where s is the sample standard deviation, N is the number of observations, x_i donated for observed values of a sample item, and $\bar{x}$ the mean value of the observations.

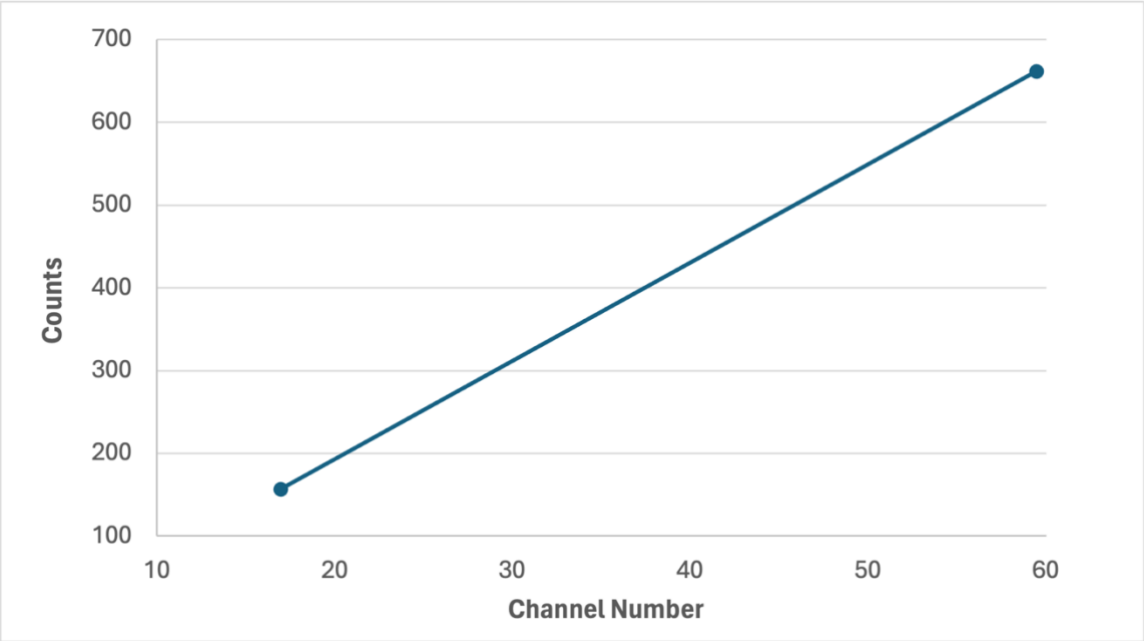

Figure 3: *Shows the data counts versus channel number. The error on the y-axis is ±15.2, which is too small to be observable.*

The equation of the line was determined to be $y = 11.882x - 45$ used in Excel. Following the calculation of the calibration constant, the peak heights for each dataset were evaluated by plotting them in Excel for high-voltage values of $0.57\ kV$, $0.60\ kV$, $0.63\ kV$, and $0.66\ kV$. Subsequently, a new graph was generated, illustrating the relationship between peak heights and high-voltage values, as shown in Figure (4).

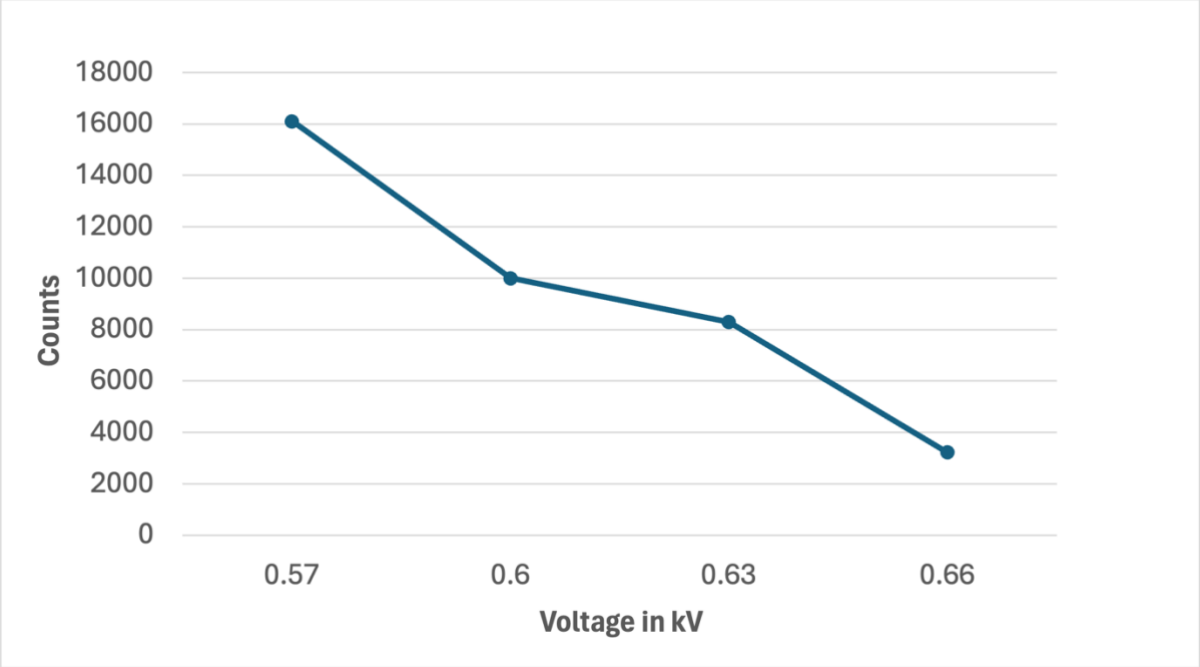

Figure 4: *The graph shows the data counts versus voltages in kV. The error on the y-axis is too small to be observable as ±158.7.*

Figure (4) demonstrates that the peak height decreases as the high voltage increases. Furthermore, the Full Width at Half Maximum (FWHM) for each high voltage was calculated, and a new graph was

generated to display the relationship between FWHM and high voltage, as shown in **Figure (5)**. This graph indicates that as the high voltage increases, the FWHM also increases.

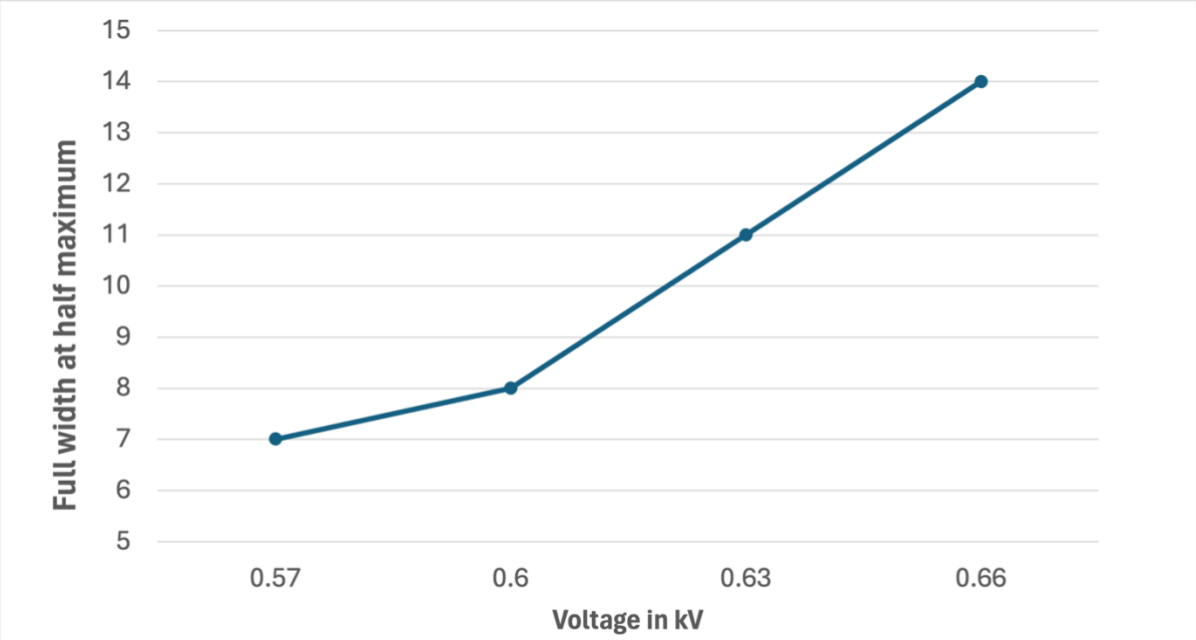

Figure 5: *The graph shows the values for FWHM as in channel numbers versus voltage in kV. The error on the y-axis is too small to be observable as ±0.02.*

The error on the y-axis was calculated by using equation(8), and using equation(9), the uncertainty of the average was calculated as 0.02 in channel numbers.

$$\Delta\bar{x} = \frac{\sigma}{\sqrt{N}} \tag{9}$$

Where $\Delta\bar{x}$ denotes the uncertainty of the average, σ is the standard deviation, and the N is the number of repeats in the investigation. Lastly, the number of counts within the photo-peak areas was calculated by summing all values between the starting and ending points of the photo-peak. A graph was then plotted to illustrate the relationship between counts in the peak area and high voltage, as shown in **Figure (6)**. This graph demonstrates that the counts per area remain nearly constant, as indicated by the linearity of the line, which neither increases nor decreases. The uncertainty of the total counts per peak area was determined by using equation(7) as 12.4 as in counts.

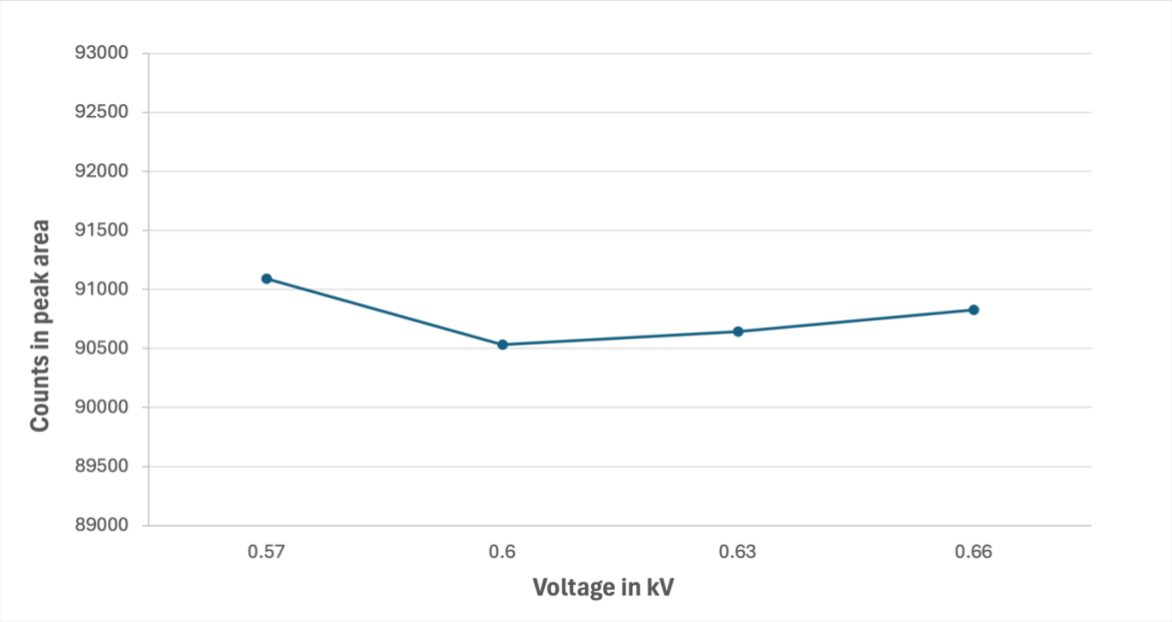

Figure 6: *Shows the data total counts in peak area versus high voltage values in kV. The error on the y-axis is too small to be observable as* $\pm$ *2063.0.*

Subsequently, the Compton scattering edge and backscattering peaks for Cs were calculated as 396.2 keV and 182.9 keV, respectively, using the calibration factor depicted in **Figure (8)**. The errors, when compared to the literature values, were determined to be 7.8% and 17.6%, respectively. Additionally, the photopeak values were identified as 609.9 keV for Cs and 49.05 keV for Am. The uncertainty of counts was determined by using equation(7) as 3.1.

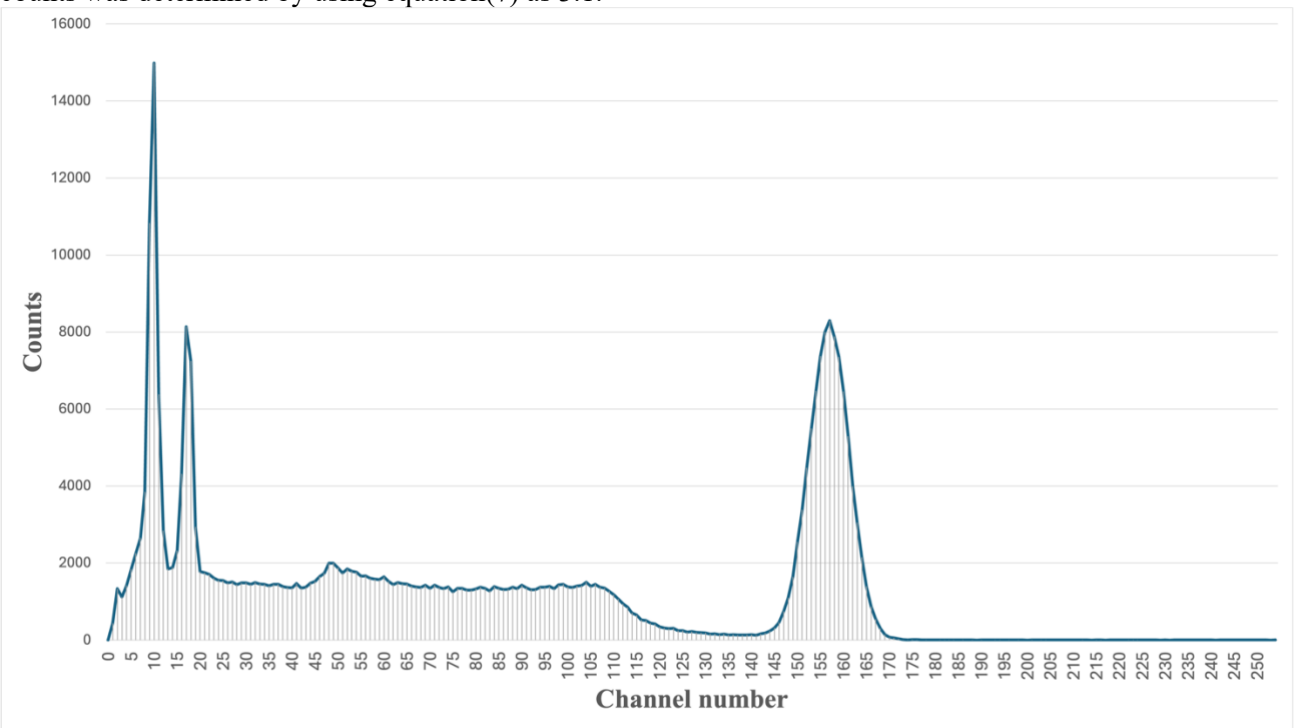

Figure 8: *Shows the data for 0.63 kV, counts in the y-axis, and channel number in the x-axis. The error on the y-axis is too small to be observedble as* $\pm$ *1882.0 .*

In the second part of the investigation, for each isotope except Am, graphs were plotted to show counts versus channel number, with each area of interest clearly labelled in the respective figures. Subsequently, gamma-peak energies were calculated using the calibration constants.

Section 2:

Figure (9) illustrates the measurement conducted for Cs-137, which has a literature peak value of 662 keV. Due to instrumental errors encountered during the investigation, the calibration constant was recalculated as 1.89 using the same methodology applied in the first part of the investigation. The photo-peak value was determined to be 761.7 keV, while the Compton scattering edge and backscattering peak were calculated as 466.3 keV and 240.3 keV, respectively. The errors associated with these experimentally determined values were calculated as 15.1% for the photo peak, 52.4% for the Compton scattering edge, and 35.2% for the backscattering peak.

Its FWHM was determined to be 49.16 keV, reflecting the detector's resolution at the photo peak. Additionally, the total count rate was calculated as 303026, indicating the overall detection efficiency for the gamma-ray emissions from Cs-137 during the measurement. The error for the number of counts was determined by using equation(7) as 4.2.

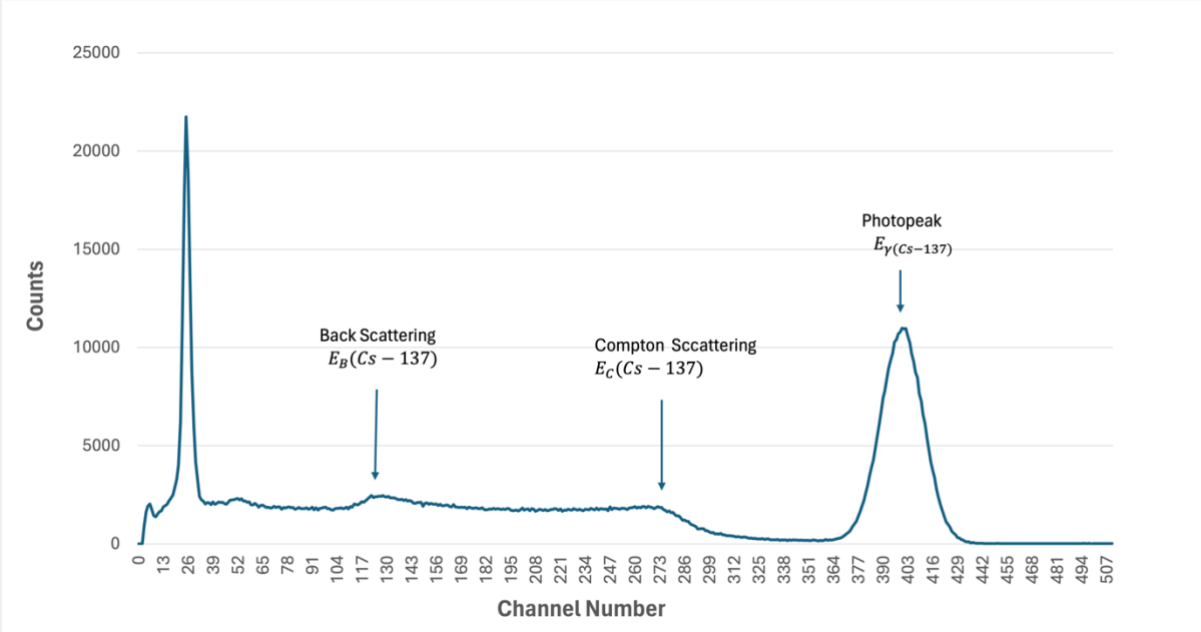

Figure 9: *Shows the data set for counts versus channel number for the isotope Cs-137.The error on the y-axis is too small to be observable as* $\pm$ *1774.2.*

For Co-60, with a literature value of 1174 keV for its photo-peak, a graph of counts versus channel number was plotted, as shown in **Figure (10)**. This graph highlights the key spectral features, including the Compton scattering edge, backscattering peak, and photopeak, providing a clear visualisation of the gamma-ray interactions and energy distribution for the isotope.

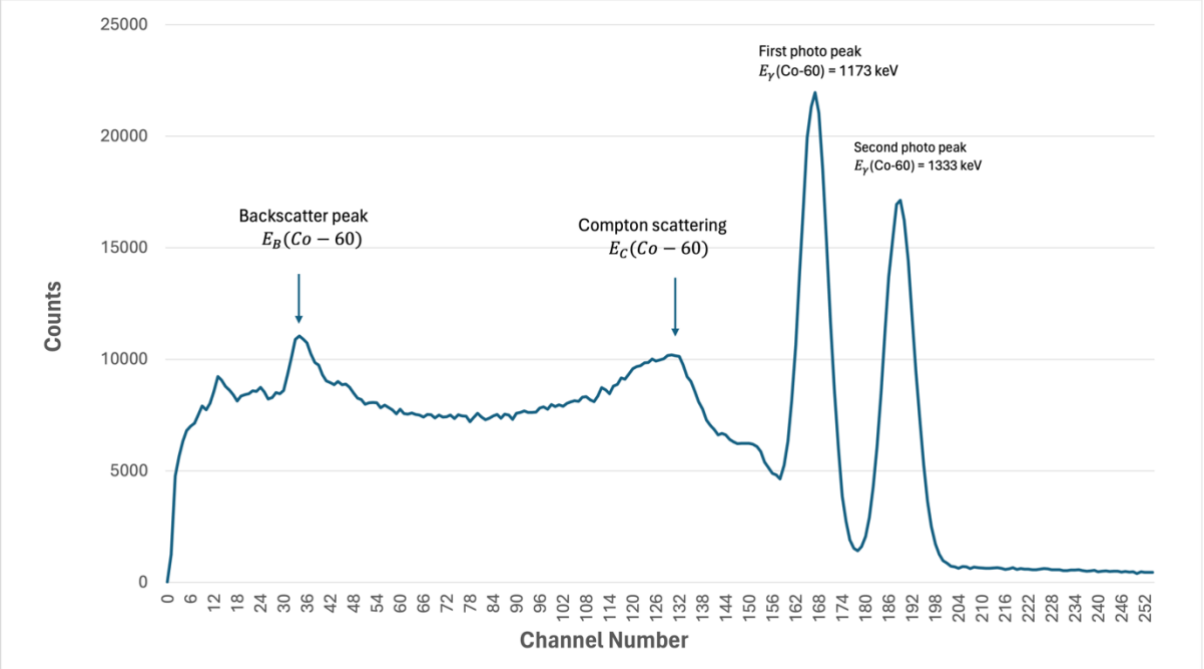

Figure 10: *Shows the data for Co-60, as counts in the x-axis and Channel number in its y-axis. The error in the y-axis is too small to be observable as* $\pm$ *1923.8.*

Due to instrumental errors encountered during the experiment, the calibration process was repeated, following the same methodology used in the first part of the investigation. The recalculated calibration constant was determined to be 7.8. Subsequently, the photopeak energy was measured as 1294 keV, and the associated error, when compared to the literature value, was calculated as 10.8%.

The Compton scattering energy was experimentally determined to be 1029 keV, and its theoretical value was calculated using equations (2), (3), and (6). A comparison of these values resulted in an error of 180%. The backscattering energy was experimentally measured as 273.0 keV, and its error was calculated based on the theoretical value, yielding an error of 71%.

The Full Width at Half Maximum (FWHM) for Co-60 was determined to be 62.4 keV. The total count in the peak area was calculated as 37725 counts, reflecting the overall detection efficiency for the gamma-ray emissions during the measurement. The error for the number of counts in the peak area was evaluated using equation (7), which was found to be 7.8%.

For Co-60, which has a literature value of 1275 keV for its photopeak, a graph of counts versus channel number was plotted, as shown in Figure (11). This graph highlights the critical spectral features, including the Compton scattering edge, backscattering peak, and photopeak, providing a detailed visualisation of the gamma-ray interactions and energy distribution for the isotope. However, the first photopeak, with a literature value of 511 keV, could not be determined experimentally as it did not appear on the graph. In this part of the analysis, no additional calibration was required, as the calibration constant from the first part of the experiment, determined to be 3.88, was utilised.

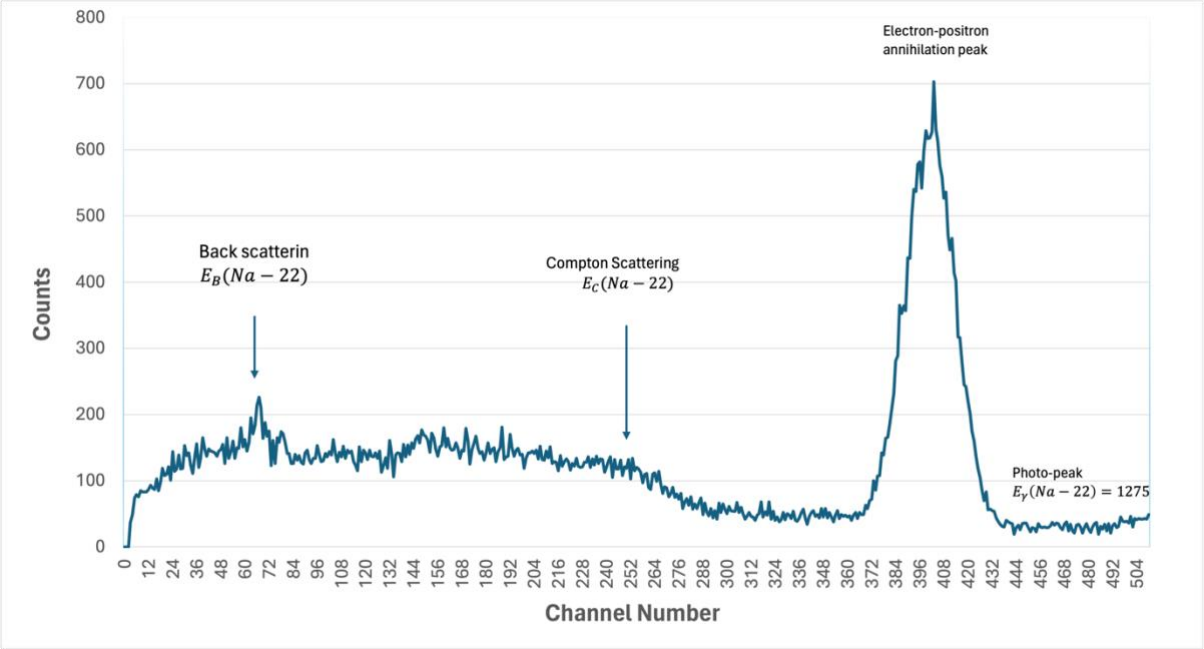

Figure 10: *Shows the data for Na-22, as counts in the x-axis and Channel number in its y-axis. The error in the y-axis is too small to be observable as* $\pm$ *58.6.*

The photopeak energy was measured as 1553 keV, and the associated error, when compared to the literature value, was calculated as 21.8%. The Compton scattering energy was experimentally determined to be 975.3 keV, and its theoretical value was calculated using equations (2), (3), and (6). A comparison of these values resulted in an error of 153%. The backscattering energy was experimentally measured as 258.0 keV, and its error was calculated based on the theoretical value, yielding an error of 50%.

The Full Width at Half Maximum (FWHM) for Na-60 was determined to be 119 keV. The total count in the peak area was calculated as 20688 counts, reflecting the overall detection efficiency for the gamma-ray emissions during the measurement. The error for the number of counts in the peak area was evaluated using equation (7), which was found to be 1.2%.

After that, the rest mass of the electron m_0c^2 was determined by using equation (3) from the calibrated spectra as 2264 keV, with compared to its literature value, the error was determined as %343.1

The photopeak does not exhibit zero width due to the detector's finite energy resolution, which arises from statistical fluctuations in the scintillator and photomultiplier tube. Additionally, system electronics, including the multichannel analyser, introduce noise. Together, these effects result in the photopeak appearing as a Gaussian distribution rather than a single sharp line.

Pair production occurs only when the gamma-ray energy exceeds 1.022 MeV, equivalent to twice the rest of the energy of the electron. Based on the results, the measured photopeak energies for the isotopes were 1298 keV for Co-60, 1553 keV for Na-22, and 761.7 keV for Cs-137. Among these, only the gamma-ray energies of Co-60 and Na-22 surpassed the critical threshold, enabling the production of positron-electron pairs within their nuclei.

The linearity of the photomultiplier was assessed by plotting photopeak energies (in keV) versus channel numbers for each isotope, as shown in **Figure (11)**. The results indicated that the

photomultiplier does not exhibit linear behaviour, as evident from the deviation of the plotted data from a linear trend.

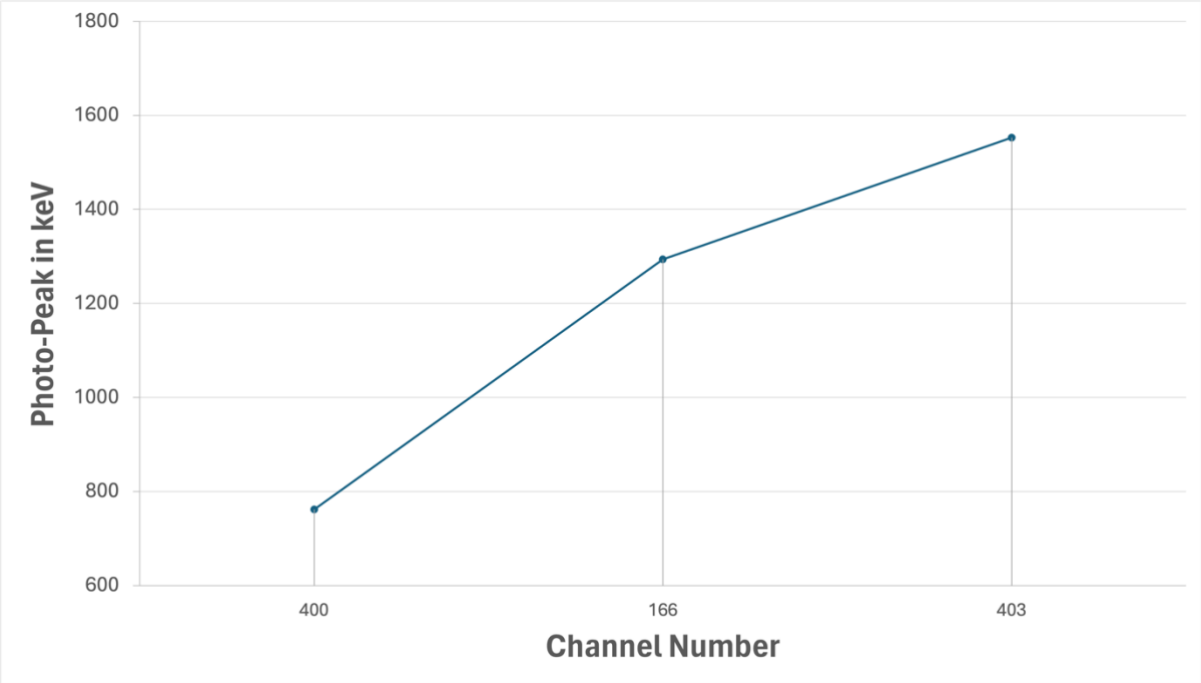

Figure 11: *Shows the data for photo-peak values in keV and channel number for isotopes Cs-137,Co-60 and Na-22.*

In the final part of the analysis, the resolution of the graph for each isotope was calculated using equation (10). To minimise errors and improve accuracy, the average resolution was subsequently determined by applying equation (7). The calculated average resolution was found to be 0.063.

Section 3:

When the voltage is set too low, the important part of the experiment cannot be distinguished by plotting graphs because when the voltage is low, the width of the peak broadens and sometimes even overlaps, which makes the results less precise. Even though if the entire graph could be plotted, in the analysis, the values will have a higher chance of being inaccurate, which would make the error on the average high.

4. Discussion

The experiment faced challenges, particularly in the calibration process, which impacted the accuracy of results. Calibration used a proportionality constant of 3.885, derived through arithmetic averaging. While this enabled gamma-ray spectra identification, repeated measurements were needed to minimize errors. Background noise subtraction improved accuracy, but systematic errors from equipment limitations persisted.

Key results included Compton scattering and backscattering peaks for Cs-137 at 396.2 keV and 182.9 keV, with errors of 7.8% and 17.6%. The electron's rest mass was calculated as 2264 keV, with a significant error of 343.1%, suggesting potential calibration issues. Higher voltages increased FWHM values, reducing resolution. Compton scattering errors for Co-60 and Na-22 were 180% and 153%,

reflecting the CSS Lab software's limitations at higher voltages. The Gaussian-shaped photopeak, influenced by statistical fluctuations and photomultiplier noise, highlighted equipment constraints. Non-linear photomultiplier behaviour, evident from deviations in plotted photopeak energies, emphasized the need for better calibration and advanced measurement techniques.

5. Conclusion

This experiment successfully demonstrated the principles of gamma-ray interactions, including Compton scattering, backscattering, and photopeak identification. The proportionality constant for calibration was determined as 3.885, and the electron's rest mass was calculated as 2264 keV, with a 343.1% error. For Cs-137, the Compton scattering edge and backscattering peaks were found to be 396.2 keV and 182.9 keV, with errors of 7.8% and 17.6%, respectively. Similarly, Co-60 and Na-22 had photopeak energies of 1294 keV and 1553 keV, with errors of 10.8% and 21.8%.

Higher voltages led to increased FWHM values, reflecting resolution limitations. Counts per peak area remained nearly constant, indicating stable detection efficiency. However, significant errors in Compton scattering and backscattering values, coupled with the photomultiplier's non-linear behaviour, highlighted the need for enhanced equipment. Future improvements, such as advanced scintillation materials or semiconductor detectors, could provide better resolution and reliability in gamma-ray spectroscopy.

References

- Department of Physics (2024) ‘5CCP2100 Experimental Physics Laboratory Manual 2024/25’. London: King’s College London.
- Molah, A. (2019) Evaluation of Gamma Radiation Attenuation Characteristics of Different Type Shielding Materials used in Nuclear Medicine Services, Compton polarimeter for 10–30 keV x rays. Available at: https://www.researchgate.net/publication/334993133_Evaluation_of_Gamma_Radiation_Attenuation_Characteristics_of_Different_Type_Shielding_Materials_used_in_Nuclear_Medicine_Services (Accessed: 22 November 2024).
- Veale, M. (2009) Charge Transport and low Temperature Phenomena in Single Crystal CdZnTe. Available at: https://www.researchgate.net/publication/236131292_Charge_Transport_and_low_Temperature_Phenomena_in_Single_Crystal_CdZnTe (Accessed: November 2024).